Plant Physiology®

CYCLIC NUCLEOTIDE-GATED ION CHANNEL 2 modulates auxin homeostasis and signaling

Sonhita Chakraborty,[1] Masatsugu Toyota [iD],[2] Wolfgang Moeder [iD],[1] Kimberley Chin,[1] Alex Fortuna,[1] Marc Champigny,[3] Steffen Vanneste [iD],[4,5,6] Simon Gilroy [iD],[7] Tom Beeckman [iD],[4,5] Eiji Nambara [iD] [1] and Keiko Yoshioka [iD] [1,8,†,*]

1 Department of Cell and Systems Biology, University of Toronto, Toronto, , Canada, ON M5S 3B2
2 Department of Biochemistry and Molecular Biology, Saitama University, Sakura-ku, Saitama, 338-8570, Japan
3 PhenoLogic Co., Toronto, Canada, ON M5A 2N1
4 Department of Plant Biotechnology and Bioinformatics, Ghent University, 9052 Ghent, Belgium
5 Faculty of Bioscience Engineering, Department Plants and Crops, Ghent University, Unit HortiCell, Coupure Links 653, 9000 Ghent, Belgium
6 Lab of Plant Growth Analysis, Ghent University Global Campus, Songdomunhwa-Ro, 119, Yeonsu-gu, Incheon 21985, Republic of Korea
7 Department of Botany, University of Wisconsin, Madison, WI 53706, USA
8 Center for the Analysis of Genome Evolution and Function (CAGEF), University of Toronto, Toronto, Canada, ON M5S 3B2

*Author for communication: Keiko.yoshioka@utoronto.ca
†Senior author.

Abstract

Cyclic nucleotide-gated ion channels (CNGCs) have been firmly established as Ca^{2+}-conducting ion channels that regulate a wide variety of physiological responses in plants. CNGC2 has been implicated in plant immunity and Ca^{2+} signaling due to the autoimmune phenotypes exhibited by null mutants of *CNGC2* in *Arabidopsis thaliana*. However, *cngc2* mutants display additional phenotypes that are unique among autoimmune mutants, suggesting that CNGC2 has functions beyond defense and generates distinct Ca^{2+} signals in response to different triggers. In this study, we found that *cngc2* mutants showed reduced gravitropism, consistent with a defect in auxin signaling. This was mirrored in the diminished auxin response detected by the auxin reporters DR5::GUS and DII-VENUS and in a strongly impaired auxin-induced Ca^{2+} response. Moreover, the *cngc2* mutant exhibits higher levels of the endogenous auxin indole-3-acetic acid, indicating that excess auxin in the *cngc2* mutant causes its pleiotropic phenotypes. These auxin signaling defects and the autoimmunity syndrome of the *cngc2* mutant could be suppressed by loss-of-function mutations in the auxin biosynthesis gene *YUCCA6* (*YUC6*), as determined by identification of the *cngc2* suppressor mutant *repressor of cngc2* (*rdd1*) as an allele of *YUC6*. A loss-of-function mutation in the upstream auxin biosynthesis gene *TRYPTOPHAN AMINOTRANSFERASE OF ARABIDOPSIS* (*TAA1*, *WEAK ETHYLENE INSENSITIVE8*) also suppressed the *cngc2* phenotypes, further supporting the tight relationship between CNGC2 and the TRYPTOPHAN AMINOTRANSFERASE OF ARABIDOPSIS–YUCCA -dependent auxin biosynthesis pathway. Taking these results together, we propose that the Ca^{2+} signal generated by CNGC2 is a part of the negative feedback regulation of auxin homeostasis in which CNGC2 balances cellular auxin perception by influencing auxin biosynthesis.

Introduction

Calcium (Ca^{2+}) is a ubiquitous second messenger that orchestrates many signaling pathways in eukaryotes. A diverse range of stimuli elicit transient changes in the cytosolic-free Ca^{2+} concentration ($[Ca^{2+}]_{cyt}$) in plants. These include developmental cues, abiotic stresses such as drought, heat, and wounding, and biotic stimuli such as interactions with pathogenic and symbiotic microorganisms (Yuan et al., 2017; Moeder et al., 2019). Each type of stimulus is thought to generate a distinctive spatio-temporal "Ca^{2+} signature", which is decoded by the direct binding of Ca^{2+} to calcium sensor proteins such as calmodulins (CaM), calcium-dependent protein kinases (CDPKs), and others (Edel et al., 2017). These sensor proteins may undergo conformational changes upon binding and interact with or phosphorylate various target substrates to regulate downstream factors (DeFalco et al., 2010; Edel et al., 2017). The Ca^{2+} flux is regulated by a combination of various channels, pumps, and transporters, which move Ca^{2+} to and from extracellular and/or intracellular Ca^{2+} stores to the cytoplasm (Demidchik et al., 2018). Despite the central role played by Ca^{2+} in plant physiological responses, the identity of plant Ca^{2+} channels that regulate specific $[Ca^{2+}]_{cyt}$ remains elusive.

Cyclic nucleotide-gated ion channels (CNGCs) function as Ca^{2+} channels and are linked to Ca^{2+} signaling in plants (Jammes et al., 2011; Zelman et al., 2012, DeFalco et al., 2016; Moeder et al., 2019; Dietrich et al., 2020). They are involved in a variety of physiological processes that are regulated by Ca^{2+} signaling, such as pollen tube growth, thermo-sensing, pathogen resistance, root growth, and symbiotic interactions (Moeder et al., 2011; Finka et al., 2012; Charpentier et al., 2016; Brost et al., 2019; Dietrich et al., 2020). The involvement of CNGCs in plant defense was first suggested in a study of the *Arabidopsis thaliana* null mutant of *CNGC2*, *defense, no death1* (*dnd1*, also known as *cngc2-1*). *cngc2* mutants exhibit autoimmune phenotypes such as stunted growth, conditional spontaneous cell death, and elevated basal levels of salicylic acid (SA), which confer enhanced resistance to various pathogens (Yu et al., 1998; Clough et al., 2000). They have a reduced ability to mount a hypersensitive response (HR), which is a form of programmed cell death around the site of pathogen infection, often observed during effector triggered immunity (Yu et al., 1998). Two null mutants of *CNGC4*, *HR-like lesion mimic1* (*hlm1*; Balagué et al., 2003) and *defense, no death2* (*dnd2*, later referred to as *cngc4*; Jurkowski et al., 2004), and a gain-of-function mutant of *CNGC12*, *constitutive expresser of pathogenesis-related genes22* (*cpr22*), also show alterations in defense responses (Yoshioka et al., 2006). The inhibition of HR-like spontaneous cell death in *cpr22* by Ca^{2+} channel blockers, and the higher $[Ca^{2+}]_{cyt}$ levels in *cpr22* further support the notion that *CNGC12* induces a defense response by activating Ca^{2+} signaling (Urquhart et al., 2007; Moeder et al., 2011, 2019). In contrast, the *cngc2* mutant displays a reduced HR phenotype and suppression of Ca^{2+} signals induced by pathogen elicitors, suggesting that CNGC2 positively regulates defense (Ali et al., 2007, Tian et al., 2019). However, the autoimmune phenotype of *cngc2* contradicts this notion (Moeder et al., 2011; Dietrich et al., 2020).

The *cngc2* mutant is hypersensitive to elevated Ca^{2+} levels (Chan et al., 2003). A genome-wide transcriptional study revealed that the gene expression pattern of *cngc2* resembles that of the wild-type (WT) under elevated Ca^{2+} stress (Chan et al., 2008). This observation was supported by a study reporting that CNGC2 maintains Ca^{2+} homeostasis by facilitating Ca^{2+} unloading from the vasculature into leaf cells (Wang et al., 2017). The Ca^{2+} hypersensitivity of *cngc2* may be the cause of the autoimmune phenotypes (high SA levels, H_2O_2 accumulation, and cell death), since these are largely suppressed when *cngc2* seedlings are grown in media with low $[Ca^{2+}]$ (Chan et al., 2003; Wang et al., 2017; Tian et al., 2019). *cngc2* mutants are impaired in pathogen-associated molecular pattern (PAMP)-induced immunity under Ca^{2+} concentrations that induce the pleiotropic phenotypes of this mutant, suggesting a complex relationship between Ca^{2+} concentration and immunity in this mutant (Tian et al., 2019).

In addition to these immunity phenotypes, multiple studies reported roles of CNGC2 in abiotic stress responses and development. For example, *cngc2* plants display delayed flowering. This is not typical for conventional SA-accumulating autoimmune mutants, which usually exhibit early flowering (Chin et al., 2013; Fortuna et al., 2015). This finding suggests that the autoimmune phenotype observed in *cngc2* may not be simply due to elevated SA levels. CNGC2 has also been suggested to play a role in CLAVATA3/CLAVATA1 (CLV3/CLV1) signaling in shoot apical meristem (SAM) maintenance (Chou et al., 2016). CLV1, a plasma membrane-localized receptor kinase, and its peptide ligand CLV3 regulate cell differentiation (Somssich et al., 2016). Most recently, CNGC2 was also implicated in light stress induced Ca^{2+} signaling (Fichman et al., 2021). Jointly, these observations indicate that CNGC2 could be activated by a diverse set of signals, feeding into immunity, stress tolerance, and developmental outputs (Dietrich et al., 2020).

The plant hormone auxin plays a central role throughout plant development and its activity is typically associated with local accumulation that triggers a developmental response (Vanneste and Friml, 2009). The most bioactive endogenous auxin, indole-3-acetic acid (IAA), is produced from tryptophan via indole-3-pyruvate in a two-step reaction, involving the TRYPTOPHAN AMINOTRANSFERASE OF ARABIDOPSIS (TAA) and YUCCA (YUC) enzyme families in Arabidopsis (Mashiguchi et al., 2011; Stepanova et al., 2011; Won et al., 2011). The YUC proteins belong to the flavin-containing monooxygenase (FMO) enzyme family and play important roles in growth and development via auxin production (Cheng et al., 2006). For example, the *yuc* mutants and *YUC* overexpression lines show defects in pollen development, embryogenesis, senescence process, and leaf

morphology (Cheng et al., 2007; Kim et al., 2011; Cao et al., 2019). In addition, *YUC* genes are involved in stress responses such as heat and drought stress as many environmental stimuli converge on this pathway to modify plant growth and development (Cao et al., 2019).

To study CNGC2-mediated signal transduction, we screened for suppressors of a *cngc2* null mutant and identified *repressor of defense, no death1* (*rdd1*; Chin et al., 2013). The *rdd1* mutation suppresses almost all *cngc2*-related phenotypes, except its Ca^{2+} hypersensitivity, indicating that *RDD1* acts downstream of CNGC2's channel function. In this study, we identified the causal mutation of *rdd1* as a loss-of-function mutation in the auxin biosynthesis gene, *YUCCA6* (*YUC6*). Here, we propose that CNGC2 plays a role in auxin homeostasis in addition to immunity as *cngc2* is defective in canonical auxin signaling and auxin-induced Ca^{2+} signaling, phenotypes that can also be all explained by hyper-accumulation of endogenous IAA.

Results

rdd1 is a loss-of-function allele of *YUC6*

The CNGC2 null mutant *dnd1* results from a point mutation. In this study as well as Chin et al. (2013), we used the *cngc2-3* T-DNA insertion knockout line (a *CNGC2* T-DNA insertion line in the Columbia background). To clone the causal locus for *rdd1*, *rdd1 cngc2-3* plants were outcrossed with *cngc2-1* (in the Wassilewskija [Ws] background) to generate a mapping population. Using 705 plants of this F_2 mapping population, the causal locus for *rdd1* was mapped to ∼800-kb region that contained 193 coding sequences (Chin et al., 2013). Using whole-genome sequencing, the causal mutation of *rdd1* was narrowed down to four candidate genes within this region: *AT5G24680*, *AT5G25590*, *AT5G25620*, and *AT5G26050*. Of these, only the mutation in *AT5G25620* was located in a coding region. Using reverse transcription quantitative polymerase chain reaction (RT-qPCR) analysis, we found that *rdd1* did not have significant alterations in the expression of the three other candidate genes (Supplemental Figure S1). Therefore, the causal mutation of *rdd1* is likely a nonsynonymous amino acid change from proline to leucine at residue 297 in the third exon of *AT5G25620*, which encodes the protein YUC6, an FMO-like protein involved in a key step in auxin biosynthesis (Figure 1A; Mashiguchi et al., 2011; Won et al., 2011). *rdd1* is a point mutation that does not cause a premature stop codon or frame shift in the *YUC6* gene. Furthermore, the *rdd1* mutation was not located in or in proximity of any of the known domains of YUC6 (Figure 1A); thus, its suppression of the *cngc2* phenotype could be due to either a gain- or loss-of-function of this enzyme. To determine which of these was the case, we tested *yuc6-1D*, a *YUC6* overexpressing activation line (Kim et al., 2007), and *yucca6-3k* (henceforth, *yuc6*), a *YUC6* knockout mutant (Cheng et al, 2006), for their ability to suppress *cngc2* phenotypes. First, we introduced the *yuc6-1D* allele into *cngc2*. None of the 132 F_2 generation plants analyzed, resulting from a cross between *yuc6-1D* and *cngc2*, showed an *rdd1*-like

morphological phenotype. Instead, we observed seedlings that had a smaller stature than either parental line (enhanced dwarfism), while displaying a typical *yuc6-1D* phenotype (such as long, narrow leaves with elongated petioles; Figure 1B, Kim et al., 2007). Thus, we genotyped the *yuc6-1D* and *cngc2* status of 47 F_2 progenies (Supplemental Table S1). We found that these smaller plants were homozygous for *cngc2* and *yuc6-1D* positive. Therefore, *yuc6-1D* does not rescue the dwarf phenotype of *cngc2*; rather, it enhances this phenotype (indicated as ss in Supplemental Table S1).

In contrast, the loss-of-function mutant *yuc6* suppressed the *cngc2* phenotype. Indeed, the *yuc6 cngc2* homozygotes in an F_2 population derived from a cross between *yuc6* and *cngc2* were identical in phenotype to *rdd1 cngc2* (Figure 1B), indicating that *rdd1* is a loss-of-function allele of *YUC6*. In addition, the *rdd1* single mutant exhibited the identical broad leaf phenotype as *yuc6*, further supporting the notion that *rdd1* is a loss-of-function allele of *YUC6* (Figure 1B). The *cngc2*-like plants were more numerous in this F_2 population than would be expected if *rdd1* (and therefore also *yuc6*) were dominant in its suppression of *cngc2* (Chin et al., 2013). Therefore, we conducted additional detailed genetic analyses using two backcrossed populations of *yuc6 cngc2* × *cngc2* and *rdd1 cngc2* × *cngc2*. We found that *rdd1* is a semidominant mutation with a dosage effect (Supplemental Tables S2 and S3 and Supplemental Figure S2). The difference from the previously published *rdd1* segregation analysis (Chin et al., 2013) is probably due to the environmental sensitivity of the penetrance of *cngc2* phenotypes. Taken together, these results show that *rdd1* is a loss-of-function mutant of *YUC6* and that the *cngc2* phenotype depends on the dose of YUC6.

cngc2 phenotypes depend on functional *YUC6*

The *cngc2* mutant phenotype is complex as it displays a range of seemingly unrelated phenotypes, all of which are suppressed in *rdd1 cngc2*, with the exception of Ca^{2+} hypersensitivity (Chin et al., 2013). Therefore, we analyzed the YUC6-dependence of the *cngc2* phenotypes. As seen in *rdd1 cngc2* (Chin et al. 2013), trypan blue staining of 4-week-old plants revealed that *yuc6 cngc2* plants exhibited less spontaneous cell death than *cngc2* plants (Figure 2A). Moreover, *yuc6 cngc2* plants partially lost the enhanced resistance of *cngc2* to the oomycete pathogen *Hyaloperonospora arabidopsidis* (*Hpa*) isolate Noco2 (Figure 2, B and C). Accordingly, increased basal levels of SA in *cngc2* were suppressed to the same degree in *yuc6 cngc2* as in *rdd1 cngc2* (Figure 2D). We also analyzed the basal SA levels of the *yuc6* single mutants multiple times and did not find a statistically significant alteration in these mutants, indicating that *yuc6* and *rdd1* epistatically suppress increased SA levels in *cngc2* (Supplemental Figure S3). Furthermore, *cngc2* exhibits delayed flowering, which is suppressed in *rdd1 cngc2* in an SA-independent manner (Fortuna et al., 2015). Like *rdd1 cngc2*, the *yuc6 cngc2* plants showed suppression of the delayed flowering and even displayed earlier flowering,
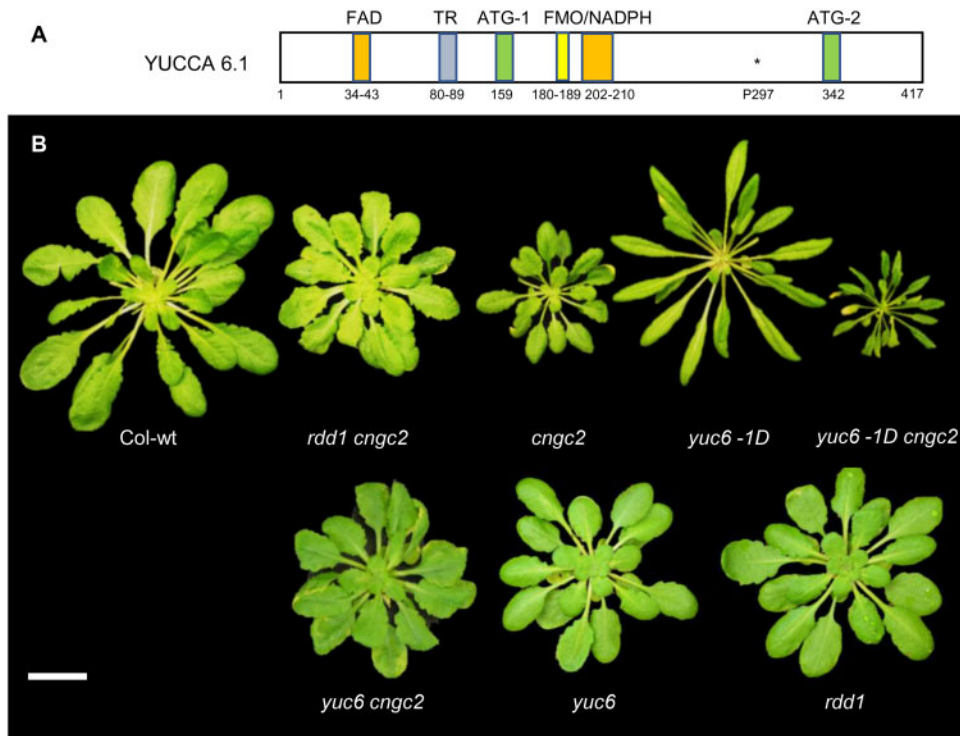
Figure 1 *rdd1* is a loss-of-function allele of *YUCCA6*. A, Schematic representation of the *rdd1* mutation and catalytic sites in YUCCA6 (YUC6). The relative locations of the FAD-binding domain (FAD, aa 34–43), thiol reductase domain (TR, aa 80–89), FMO identity sequence (FMO, aa 180–189), and NADPH-binding domain (NADP, aa 202–210), the ATG-containing motifs (ATG1, aa 159; ATG2, aa 342), and the *rdd1* mutation position P297 are depicted based on gene model YUC6.1 TAIR). B, Morphology of approximately 5-week-old plants grown in short day conditions (9L:15D). *yuc6 cngc2* partially suppress *cngc2*-conferred dwarf morphology to the same degree as *rdd1 cngc2*. *yuc6*, the YUC6 knockout line, has shorter and wider rosette leaves compared to Col-wt, similar to the *rdd1-1* single mutant. *yuc6-1D* is unable to suppress *cngc2*-conferred dwarf phenotypes. Yellowing of leaf tip is observed in *yuc6-1D cngc2*. Scale bar = 1 cm.

compared to the WT (Figure 2E). Taking these results together, we conclude that a wide range of *cngc2* phenotypes, including enhanced pathogen resistance, depend on functional *YUC6*.

CNGC2 negatively affects TAA1/YUC6-mediated auxin biosynthesis

Since *rdd1* is a loss-of-function allele of *YUC6*, we postulated that auxin homeostasis is mis-regulated in *cngc2* mutants. In line with our expectations, *cngc2* contained more endogenous IAA than the WT control, in shoots and roots in mature plants, and this was partially reversed in the *rdd1 cngc2* and *yuc6 cngc2* double mutants (Figure 3). This observation was statistically significant in shoots, but not in roots; however, the same trend has been observed in roots repeatedly. Thus, we think the difference between shoot and root samples is due to technical difficulties to collect mature plant root samples. This corroborates the enhanced dwarfism of *yuc6-1D cngc2* plants as *yuc6-1D* also hyper-accumulates auxin (Figure 1). These results are consistent with CNGC2 negatively affecting YUC6-dependent auxin biosynthesis/homeostasis.

To discriminate between a YUC6-specific effect and a general, auxin biosynthesis-related effect, we assessed the requirement for another auxin biosynthetic gene, *TAA1*. The *TAA1*

loss-of-function allele *weak ethylene insensitive 8* (*wei8-1*) exhibits gravitropic defects and its allelic mutant of *CK-INDUCED ROOT CURLING 1* (*ckrc1*) additionally exhibits reduced IAA levels, due to defects in the production of the substrate of YUCCAs for IAA biosynthesis (Stepanova et al., 2008; Mashiguchi et al., 2011; Zhou et al., 2011). We generated *wei8-1 cngc2* double mutants to assess the dependence of *cngc2*-associated phenotypes on IAA biosynthesis. These double mutants exhibited a similar suppression of *cngc2* phenotypes as *rdd1 cngc2* (Figure 4A) and suppressed the elevated SA levels of *cngc2* (Figure 4B). Similar to *rdd1*, *wei8-1* also partially rescued the delayed flowering of *cngc2* (Figure 4, C and D). Taken together, these data support the hypothesis that a wide variety of *cngc2* phenotypes depend on hyperactive auxin biosynthesis, rather than YUC6 function itself.

RDD1 antagonizes CNGC2-dependent auxin signaling

The *rdd1* mutation suppresses almost all *cngc2* mutant phenotypes (Chin et al., 2013). Morphological defects of *cngc2* that differ from phenotypes of other SA-related mutants suggest alterations in hormones related to development, such as auxin. Thus, we investigated the auxin-related phenotypes of *cngc2* and the *rdd1 cngc2* double mutant.
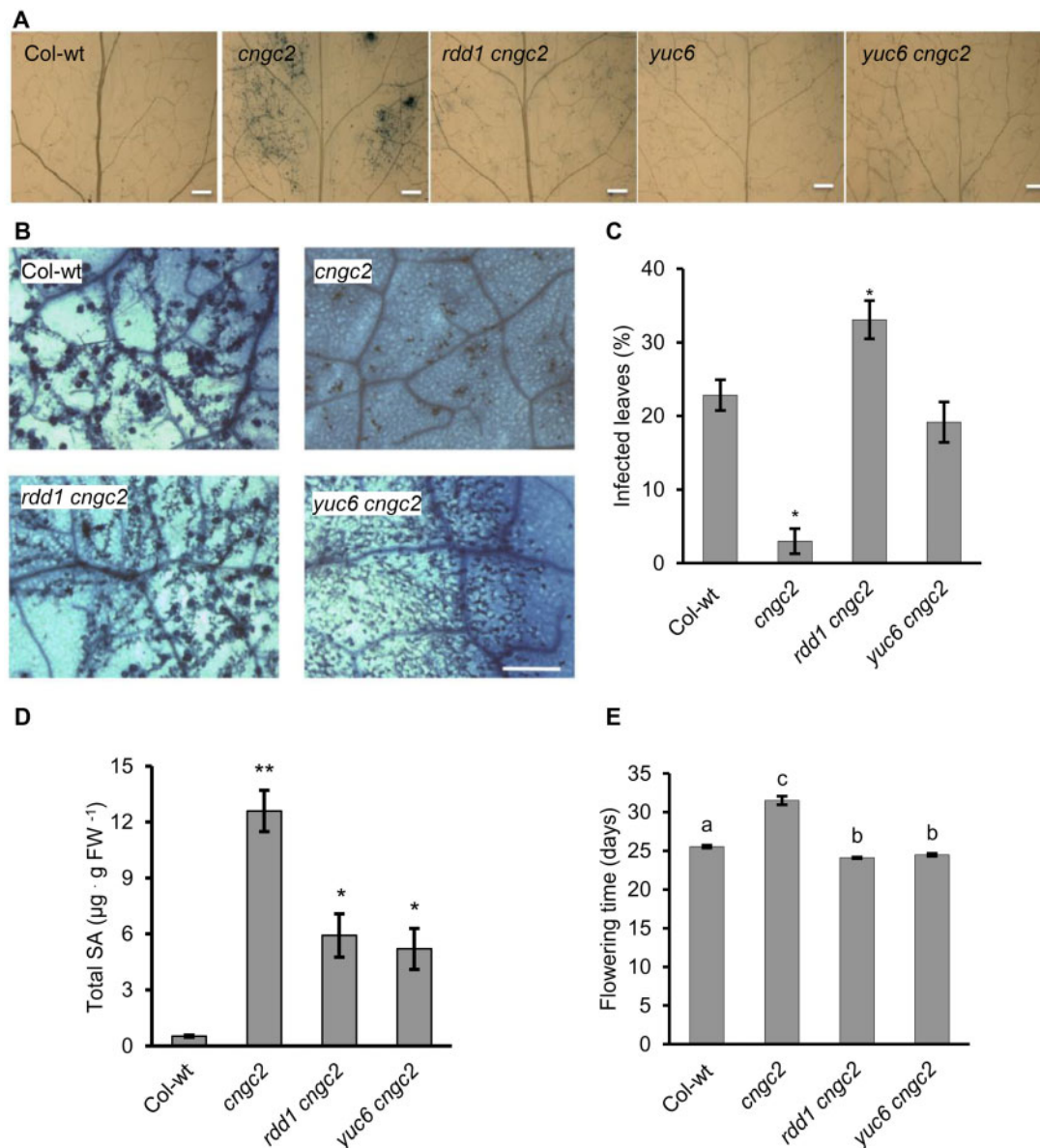
Figure 2 *yuc6* suppresses *cngc2*-conferred phenotypes. A, Trypan blue staining reveals a reduction in spontaneous cell death in *yuc6 cngc2 and rdd1 cngc2* compared to *cngc2*. Scale bar = 0.5 mm. B, Breakdown of enhanced resistance phenotype of *cngc2* in *rdd1 cngc2* and *yuc6 cngc2* double mutants upon infection with Hpa, isolate Noco2. Trypan Blue staining of Col-wt and mutants after inoculation with Hpa at a suspension of 8×10^5 spores mL^{-1}. Bar = 1 mm. C, Disease severity as a percentage of leaves showing symptoms of sporangiophore formation. Bars marked with an asterisk indicate significant difference from Col-wt (Student's *t* test, $P < 0.05$). $n = 6$. D, Total SA levels in 3- to 4-week-old WT and mutant leaves. SA levels are significantly different in *rdd1 cngc2* and *yuc6 cngc2* from *cngc2*. Error bars indicate standard error of the mean of three replicates. Bars marked with an asterisk indicate significant difference from Col-wt (Student's *t* test, $P < 0.05$). The experiment was repeated three times. E, *rdd1* and *yuc6* repress the delayed flowering phenotype of *cngc2*. *cngc2* plants exhibit delayed flowering compared to Col-wt, *rdd1 cngc2* and *yuc6 cngc2*. Shown are averages ± sᴇ, $n = 20$–32. Bars marked with the same letter indicate no significant difference (Student's *t* test, $P < 0.05$).

We found a delayed gravitropic root tip bending response in *cngc2*, which was partially rescued in *rdd1 cngc2* especially at earlier time points before 10 h (Figure 5A). We then analyzed the expression of the canonical auxin signaling output reporter, DR5 fused to GUS (DR5::GUS), as well as the Aux/IAA-based TIR1/AFB-activity sensor, DII-VENUS (Ulmasov et al., 1997; Brunoud et al., 2012). Auxin treatment elicited a strong auxin-responsive induction of DR5::GUS activity in Col-wt but not in *cngc2* roots (Figure 5B). This indicates

that the transcriptional auxin response is impaired in *cngc2*. Importantly, the *rdd1* mutation nearly completely restored the auxin responsiveness of DR5::GUS in *rdd1 cngc2* roots (Figure 5B), suggesting that RDD1 is involved in the control of auxin signaling by CNGC2.

Auxin activates DR5::GUS activity through the TIR1/AFB-dependent ubiquitination of Aux/IAA proteins and their subsequent proteolysis. Therefore, we monitored the activity of the TIR1/AFB co-receptor via the Aux/IAA degradation
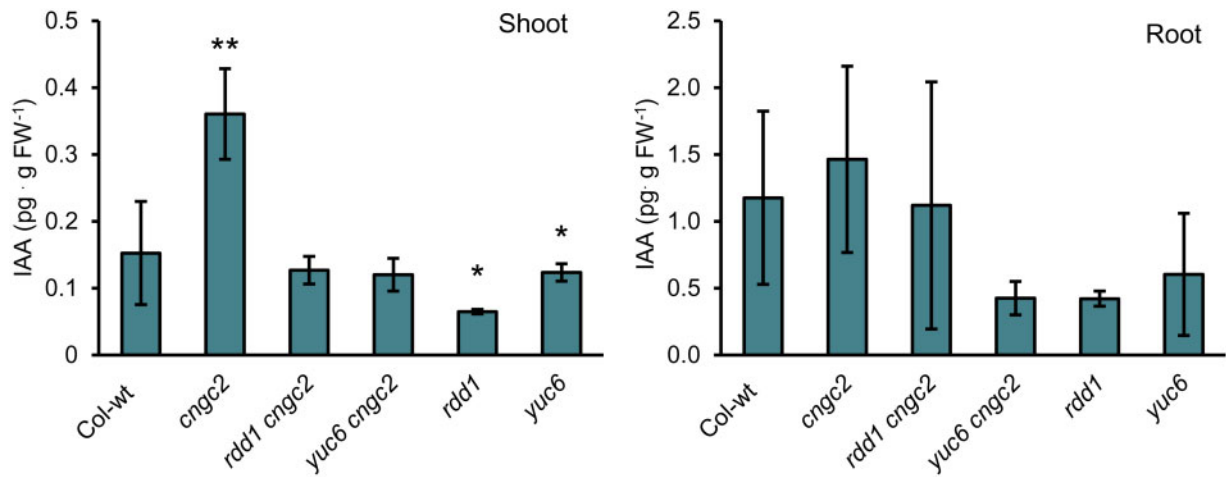
Figure 3 CNGC2 negatively affects TAA1/YUC6-mediated auxin biosynthesis. Shoot and root IAA levels of 5-week-old plants were measured using LC-MS/MS. The experiment was repeated four times and averages from one representative trial are presented; shown are ± SE, $n = 3$. Bars marked with an asterisk indicate significant difference from Col-wt (Student's t test, $P < 0.05$).
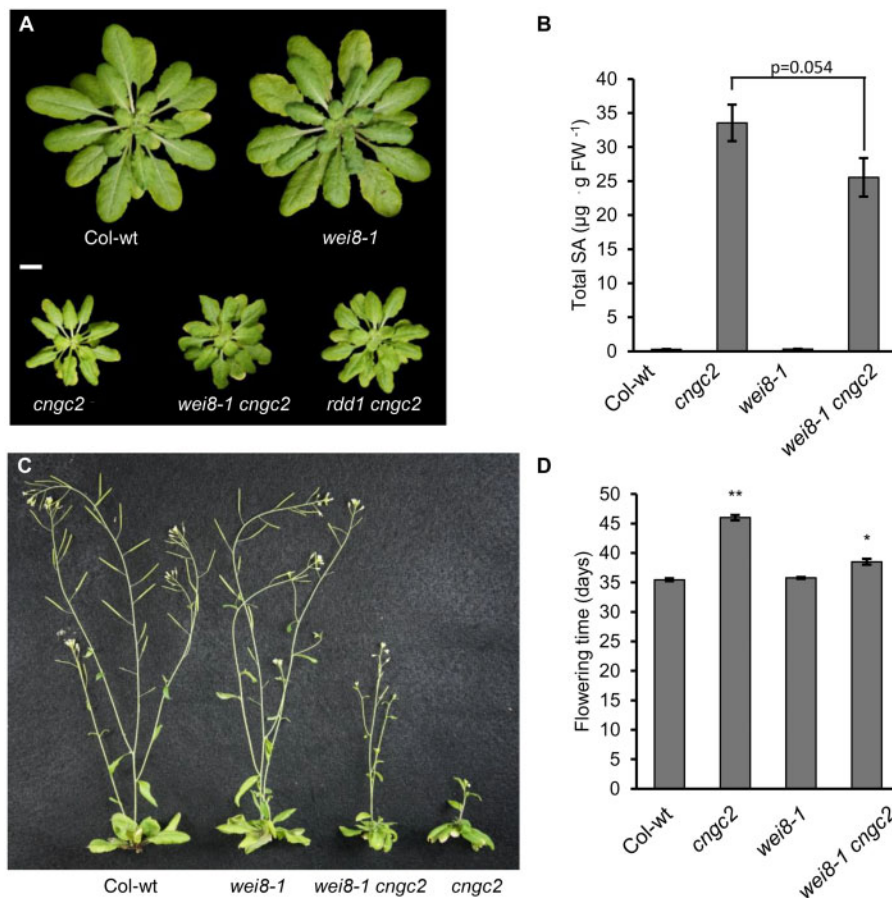

Figure 4 *wei8-1* (*taa1*) partially suppresses *cngc2*-conferred phenotypes. A, Morphology of 5-week-old Col-wt and mutant plants grown in short day conditions (9L:15D). *wei8-1 cngc2* partially suppress *cngc2*-conferred dwarf morphology to the same degree as *rdd1 cngc2*. Scale bar = 1 cm. B, Total SA levels in 5- to 6-week-old Col-wt and mutant leaves. Error bars indicate standard error of the mean of 3 replicates. C, *wei8-1* represses the delayed flowering phenotype of *cngc2*. Picture was taken at 48 d. D, Time to flowering is partially delayed in *wei8-1 cngc2*. Flowering time was measured in Col-wt and mutants by determining the emergence of the first bud. *cngc2* plants exhibit delayed flowering compared to Col-wt and *wei8-1*. Shown are averages ± SE, $n = 23$. Bars marked with an asterisk indicate a significant difference from Col-wt (Student's t test, $P < 0.05$).
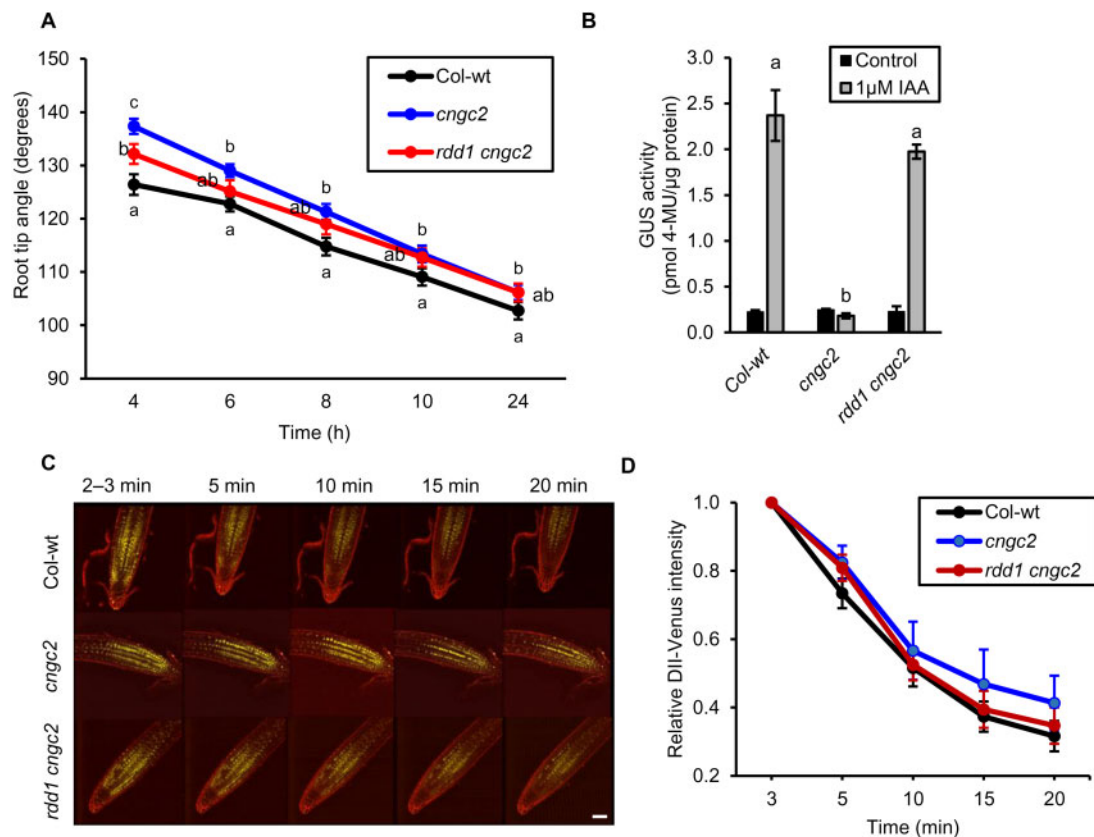
Figure 5 *cngc2* exhibits alterations in auxin-sensitivity, which is partially rescued in *rdd1 cngc2*. A, *cngc2* exhibits a delay in its gravitropic response. Time-course of gravitropic response of 7-d-old seedlings measured every 2 h from 4 h till 24 h after rotating the plate by 90°. *cngc2* displays delayed gravitropic root bending compared to the WT (Col-wt) this is partially recovered in *rdd1 cngc2*. Shown are averages $\pm$ SE (n = 10–15). Data points marked with the same letter indicate no significant difference (Student's *t* test, $P < 0.05$). B, GUS activity of DR5::GUS transgenic plants (Col-wt, *cngc2*, *rdd1 cngc2*). *cngc2* is insensitive to the application of 1µM exogenous IAA to its roots. This insensitivity is completely rescued in *rdd1 cngc2* root. Shown are averages $\pm$ SE, n = 3. Bars marked with the same letter indicate no significant difference (Student's *t* test, $P < 0.05$). C, DII:VENUS fluorescence of the primary root after the addition of 1µM IAA. (Left) Shown are representative images. (Right) Quantification of signal intensity of DII:VENUS at region of interest, relative to two minutes after the addition of 1-µM IAA. Degradation of VENUS signal is delayed in *cngc2* relative to Col-wt and *rdd1 cngc2*. Shown are averages $\pm$ SE, n = 5. All experiments were repeated three times with comparable results. Scale = 50 µm.

sensor DII-VENUS (Brunoud et al., 2012). Auxin treatment triggered rapid decay in the DII-VENUS signal over a 20-min period in 5-d-old roots in the Col-wt. This decay was slower and dampened in the *cngc2* background and was partially rescued in *rdd1 cngc2* roots (Figure 5C). Collectively, these results suggest that functional CNGC2 is required for TIR1/AFB-mediated auxin signaling. Moreover, the consistent suppression of the *cngc2* auxin-insensitivity implicates *RDD1* as a negative regulator of CNGC2 signaling.

CNGC2 is required for auxin-induced Ca^{2+} signaling in the root

A nontranscriptional branch of $SCF^{TIR1/AFB}$-based auxin perception triggers Ca^{2+} entry into the cell in a CNGC14-dependent manner (Shih et al., 2015; Dindas et al., 2018). Given that CNGC2 is required for $SCF^{TIR1/AFB}$ activity in the context of transcriptional auxin signaling, we predicted a defect in auxin-induced Ca^{2+} signaling in *cngc2*. Therefore, we

analyzed the auxin-induced Ca^{2+} response in the WT, *cngc2*, and the *rdd1 cngc2* double mutant.

The highly sensitive Förster Resonance Energy Transfer (FRET)-based Ca^{2+} sensor Yellow Cameleon (YC)-Nano65 (Choi et al., 2014) responded rapidly to auxin treatment at various regions of interest (ROI) along the root (Figure 6B). Auxin treatment at the tip of WT roots rapidly induced a strong peak in $[Ca^{2+}]_{cyt}$, followed by a more sustained Ca^{2+} response (ROI1, Figure 6, A and C). The peak response was less pronounced in more shootward ROIs (ROI2, ROI3, and ROI4), but was followed by a clear sustained Ca^{2+} response over at least 120 s. This observation in the WT was in line with previous reports using other Ca^{2+} reporters (Monshausen et al., 2011; Shih et al., 2015; Waadt et al., 2017). However, the Ca^{2+} increase upon auxin treatment was much weaker in *cngc2*. This defect was largely recovered in *rdd1 cngc2* (Figure 6, A and C). The application of cold water elicited identical Ca^{2+} signals in the WT and *cngc2*, indicating that the
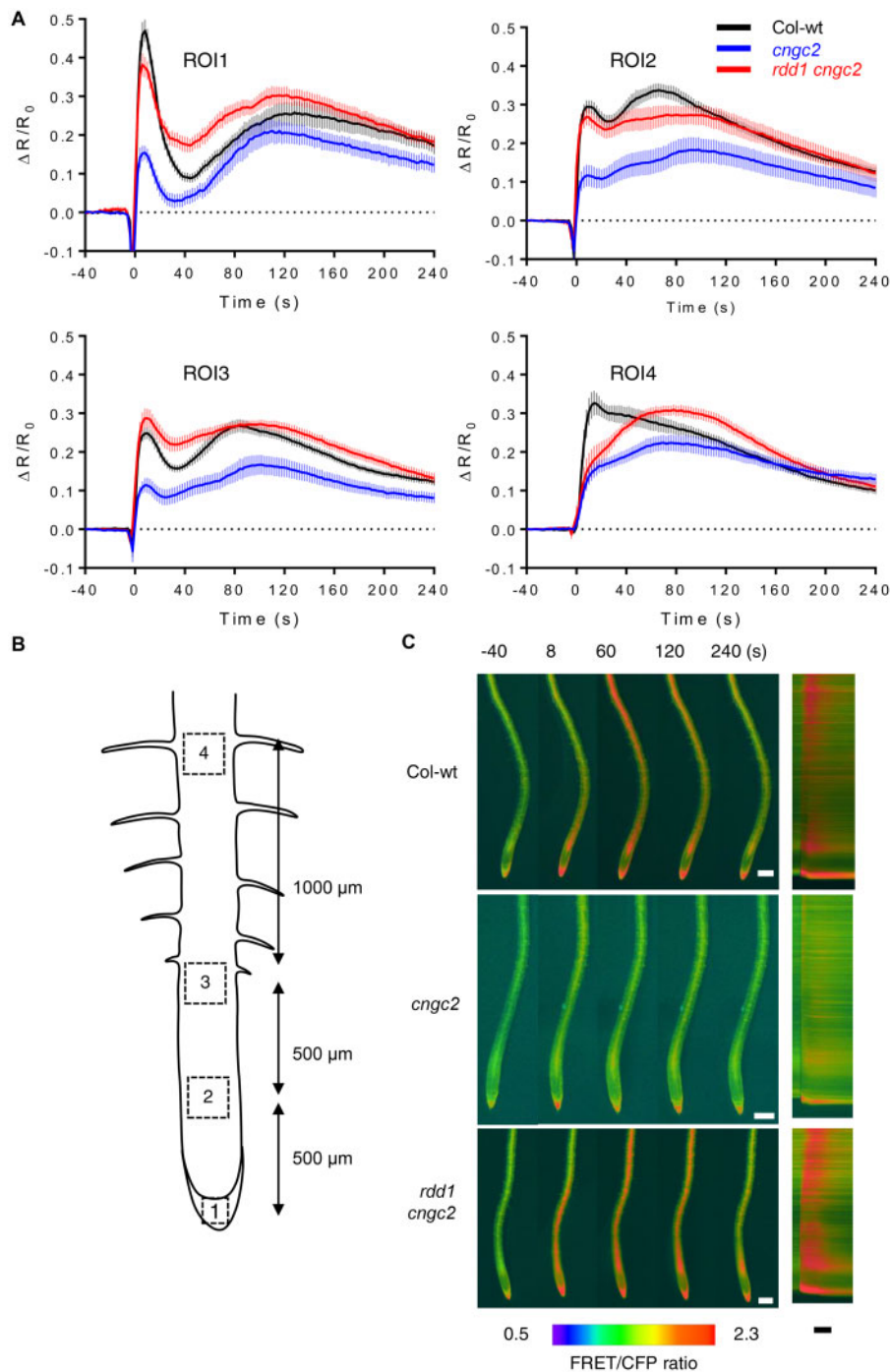
Figure 6 Auxin-mediated Ca^{2+} signals are defective in *cngc2* but rescued in *rdd1 cngc2*. A, Quantitative analysis using the FRET based Ca^{2+} sensor YCNano-65. The application of 1-μM IAA at 0 s induces Ca^{2+} spikes in columella cells (ROI1), the elongation zone (ROI2 and ROI3) and the maturation zone (ROI4) of Col-wt root, but not in these corresponding regions of *cngc2*. This is largely recovered in *rdd1 cngc2* ($n = 10–12$). B, Schematic of ROIs of the *A. thaliana* root that was examined for auxin-induced Ca^{2+} signals. 1-μM IAA was applied to the root tip region around ROI1. C, Kymograph analysis of changes in FRET/CFP ratio upon the addition of 1μM IAA in whole root of transgenic lines expressing YC-Nano65 in Col-wt, *cngc2* and *rdd1 cngc2* background. White scale bar = 0.2 mm, black scale bar = 100 s. Movies are included as a supplemental data.

impairment in IAA-induced Ca^{2+} signals in *cngc2* is not related to a general disruption of Ca^{2+} signaling (Supplemental Figure S4). Taken together, these data demonstrate a requirement for CNGC2 in auxin-mediated Ca^{2+} signaling that is dependent on RDD1.

Discussion

In the two decades since the discovery of the autoimmunity phenotype of *CNGC2* loss-of function mutants, CNGC2 has been the most intensively studied plant CNGC. However, *cngc2* exhibits pleiotropic phenotypes, which are unique

among conventional immunity mutants (Moeder et al., 2011, 2019). This indicates its wider physiological role beyond immunity and raises the fundamental question of whether a specific plant CNGC can generate different downstream signals depending on stimuli (Dietrich et al., 2020). To examine this question, we embarked on a suppressor screen of *cngc2* and discovered an unexpected, tight connection between CNGC2 and auxin biosynthesis and signaling.

CNGC2 suppresses SCF$^{TIR1/AFB}$-mediated auxin signaling

Auxin perception through the well-described SCF$^{TIR1/AFB}$-based system activates transcription by proteolysis of Aux/IAA proteins (Leyser, 2018)). Upon auxin treatment, the SCF$^{TIR1/AFB}$ receptor also activates CNGC14 via an unknown mechanism (Shih et al., 2015; Dindas et al., 2018). Here, we show that CNGC2 is required for SCF$^{TIR1/AFB}$ auxin signaling at the level of transcriptional regulation (DR5::GUS reporter analysis), as well as the induction of Ca^{2+} signals. This is reflected in the reduced root gravitropism observed in the *cngc2* mutant.

Since CNGCs were suggested to form heterotetrameric channels (Chin et al., 2013; Pan et al., 2019; Tian et al., 2019) and CNGC14 plays a role in auxin-related Ca^{2+} signaling (Shih et al., 2015; Dindas et al., 2018), it is possible that CNGC2 and 14 form a functional Ca^{2+} channel conducting auxin-induced Ca^{2+} influxes. Indeed, both CNGC14 and CNGC2 localize at the plasma membrane and are required for auxin-induced Ca^{2+} influx into the cytosol from the extracellular apoplastic Ca^{2+} pool (Lemtiri-Chlieh and Berkowitz, 2004; Shih et al., 2015; Wang et al., 2017; Dindas et al., 2018). Moreover, the gravitropic response defects of *cngc2* and *cngc14* were quite similar under our experimental conditions (Supplemental Figure S5A). However, in contrast to the pleiotropic developmental defects seen in *cngc2* (Clough et al., 2000), *cngc14* exhibits little to no additional developmental defects besides the reduced gravitropism and root hair phenotypes (Shih et al., 2015; Dindas et al., 2018; Brost et al., 2019). An additional obvious difference from *cngc2* mutants is the absence of defense-related phenotypes in *cngc14* (Shih et al., 2015; Brost et al., 2019; Dindas et al., 2018). These differences together with the limited overlap in expression patterns (Supplemental Figure S5B) indicate that CNGC14 and CNGC2 likely have different biological functions and argues against CNGC2 being a component of the SCF$^{TIR1/AFB}$-CNGC14 module and/or forming a heterotetrameric channel with CNGC14. Therefore, we favor a scenario in which CNGC2-mediated Ca^{2+} signals control auxin biosynthesis and the activity of SCF$^{TIR1/AFB}$-auxin sensing independent from CNGC14. This also provides a straightforward explanation for the reduced auxin sensitivity of DR5::GUS and DII-VENUS auxin reporters in *cngc2*.

CNCC2–CNGC4-mediated Ca^{2+} signaling suppresses auxin biosynthesis

Whether CNGC2 can form a heterotetramer with CNGC14 remains to be seen; however, CNGC2 is known to form a functional Ca^{2+} channel through heteromerization with CNGC4 (Chin et al., 2013, Tian et al., 2019). The respective mutants, *cngc2* (*dnd1*) and *cngc4* (*hlm1/dnd2*) have identical morphological and molecular phenotypes. To date, these phenotypes have mainly been characterized with respect to their autoimmunity phenotypes (Clough et al., 2000, Balagué et al., 2003), and were recently shown to be defective in PAMP-induced Ca^{2+} signals (Tian et al., 2019). Here, we found that *cngc2* exhibits hyper-accumulation of endogenous IAA similar to *cngc4* (Kale et al., 2019). This observation indicates that a CNGC2–CNGC4 heteromeric channel generates a Ca^{2+} signal that suppresses IAA biosynthesis. The auxin hyperaccumulation in *cngc2*, and most of its pleiotropic phenotypes, could be repressed when the auxin biosynthesis gene *YUC6* was mutated. Moreover, the phenotypes of *cngc4* and even the double mutant *cngc2 cngc4* could also be suppressed by the *yuc6* allele *rdd1* (Chin et al., 2013), suggesting that our findings about auxin signaling and biosynthesis in *cngc2* can be extrapolated to *cngc4*.

In addition to its FMO function for IAA biosynthesis, YUC6 also exhibits thiol reductase activity, which plays a role inReactivve Oxygen Species (ROS) homeostasis (Cha et al., 2015, 2016). Since hyper-accumulation of ROS is a common phenomenon associated with many lesion mimic mutants, including *cngc2*, it is possible that the thiol reductase activity rather than the FMO function of YUC6 is related to the suppression of *cngc2* phenotypes. However, the *rdd1* mutation is not located in the thiol reductase domain (Figure 1A). Furthermore, loss-of-function of TAA1/WEI8, which functions one step upstream of YUC6 in the IAA biosynthesis pathway, also rescues *cngc2* phenotypes. This strongly suggests that alterations in IAA biosynthesis, not the thiol reductase activity of YUC6, lead to the suppression of *cngc2*. The *taa1* (*wei8-1*) mutation had a slightly weaker effect on *cngc2* than *yuc6*, probably due to redundancies with TRYPTOPHAN AMINOTRANSFERASE-RELATED PROTEIN 1 and 2 (TAR1, TAA2; Stepanova et al., 2008). Taken together, the unique morphological and physiological phenotypes of *cngc2* and *cngc4* among lesion mimic mutants can be explained by a hyperactive TAA–YUC auxin biosynthesis pathway. Indeed, other lesion mimic mutants such as *suppressor of npr1-1, constitutive1* (*snc1*) and *constitutive expressor of PR genes 6* (*cpr6*) exhibit lower levels of endogenous IAA (Wang et al., 2007), further supporting this notion. Recently, auxin perception via the TRANS-MEMBRANE KINASE 4 (TMK4) receptor-like kinase was shown to suppress auxin biosynthesis via phosphorylation of TAA1 (Wang et al., 2020). Therefore, it will be interesting to see if TMK4 acts together with CNGC2 to suppress auxin biosynthesis.

CNGC2-mediated Ca^{2+} signals at the nexus of immunity and development

As mentioned, the autoimmunity mutants *cngc2* and *cngc4* have almost identical phenotypes including elevated SA levels, which are suppressed by *rdd1* (Chin et al., 2013). Thus, the identification of *RDD1* as the auxin biosynthesis gene

YUC6 initially led us to hypothesize that the effect of *rdd1* is simply restoring the balance in the SA–auxin antagonism in *cngc2*. Auxin treatment promotes disease symptoms and prevents the full induction of the SA-inducible antimicrobial gene *PATHOGENESIS RELATED1* (*PR1*), indicating that auxin antagonizes defense responses via suppression of SA signaling. Indeed, many pathogenic microorganisms manipulate plant immunity through modification of auxin signaling by their effectors and/or auxin originating from the microorganisms themselves (Mutka et al., 2013; Kazan and Lyons, 2014; Kunkel and Harper, 2018). Moreover, treatment with SA or the SA analog BTH globally suppresses transcription of auxin-related genes and various autoimmune mutants exhibit lower IAA levels and reduced sensitivity to auxin (Wang et al., 2007). However, the *cpr22* autoimmune phenotype, caused by the *CNGC11/12* gain-of-function mutation, which induces constitutive activation of Ca^{2+} signals (Moeder et al., 2019), was not suppressed by *rdd1* (Fortuna et al., 2015). Furthermore, blocking SA biosynthesis by introducing the *SALICYLIC ACID INDUCTION DEFICIENT 2* (*sid2*) mutation reverted almost all phenotypes of *cpr22* (Yoshioka et al., 2006), while the *sid2 cngc2* and *sid2 cngc4* double mutants retain clear morphological defects (Genger et al., 2008). Thus, simple SA–auxin antagonism is not the cause of the suppression of *cngc2* and *cngc4* phenotypes by *rdd1*.

These data also suggested that CNGC2/CNGC4 activate autoimmunity through distinct pathways, indicating a unique aspect in CNGC2/CNGC4-mediated immunity among lesion mimic mutants. Thus, *CNGC2* may primarily play a role in auxin homeostasis/signaling and its observed immunity phenotypes (i.e. SA accumulation) are a consequence of this auxin-related defect. Alternatively, *CNGC2* may act independently or at a pivotal point in multiple physiological processes, such as defense and development. Indeed, *CNGC2* has recently been implicated in the regulation of SAM size through the CLAVATA signaling cascade and Ca^{2+} homeostasis (Chou et al., 2016; Wang et al., 2017) as well as PAMP-induced immunity (Tian et al., 2019). Ca^{2+} is a universal secondary messenger and is involved in almost all aspects of cellular signaling. It is possible that CNGC2 generates distinct Ca^{2+} signals (or Ca^{2+} signatures) depending on the stimulus and acts at the nexus of immunity and development. Such specificity could be achieved through changing channel subunit composition or by being part of a channelosome with stimuli-specific signaling components, such as receptors and decoders (Dietrich et al., 2020).

Taking our results together, we propose that plasma membrane localized CNGC2 forms a heterotetrameric channel with CNGC4 and generates Ca^{2+} signals that affect the TAA–YUC auxin biosynthetic pathway, likely to prevent the overaccumulation of IAA. CNGC4 has been reported to form a heterotetramer with CNGC2 (Chin et al., 2013, Tian et al., 2019) and *cngc4* also exhibits abnormal accumulation of IAA (Kale et al., 2019). Since the loss-of-function mutants of CNGC2 are impaired in their ability to generate a Ca^{2+} influx upon IAA treatment, the regulation of the TAA–YUC

auxin biosynthetic pathway by CNGC2/CNGC4 must be a feedback regulation for auxin homeostasis, similar to that proposed by Wang et al. (2020) for TMK4. In addition, CNGC2 function is required for TIR/AFB-mediated auxin signaling; thus, CNGC2/4-mediated Ca^{2+} signals may control the activity of $SCF^{TIR1/AFB}$-auxin sensing directly, or via facilitating proper IAA homeostasis. In this scenario, *cngc2* has abnormal accumulation of IAA resulting in the desensitization of cellular auxin signaling and morphological defects as a long-term effect. Alternatively, Ca^{2+} signals generated by CNGC2 may directly affect auxin signaling in addition to its biosynthesis. In any case, CNGC2 must play a role immediately after perception of auxin or associated to the perception itself. Although at this point, we cannot exclude other possibilities such as indirect effects, this model can be one plausible scenario. Further investigation of direct downstream targets of CNGC2-mediated Ca^{2+} influx will be necessary.

For two decades, CNGC2 has been studied intensively from an immunity point-of-view. However, publications in recent years as well as our current work strongly indicate a more diverse range of functions for CNGC2. Thus, the current study contributes to a more comprehensive understanding of CNGC2-mediated Ca^{2+} signaling and reveals the importance of CNGC2 beyond its role in defense.

Materials and methods

Plant materials and growth conditions

For phenotypic analyses, *A. thaliana* seeds were cold stratified at 4°C for 2 d prior to being grown at 23°C on Sunshine-Mix #1 (Sun Gro Horticulture, Vancouver, Canada). Plants were grown in a growth chamber with a 9-h photoperiod (9-h light/15-h dark) and a day/night temperature regime of 22°C/18°C. This condition prolongs the growth stage and induces clearer morphological phenotypes of the mutants. For other experiments, plants were grown on Petri dishes with half-strength Murashige and Skoog (1/2 MS) medium, 1% sucrose (w/v), and 0.8% (w/v) agar at pH 5.8 under ambient light conditions. Sterile media was either supplemented with IAA of the desired concentration or equal volumes of ethanol as a solvent control. Homozygous mutants were identified by PCR using primers listed in Supplementary Table S4. Since *rdd1* was isolated using the T-DNA insertion allele *cngc2-3* (Chin et al., 2013), we used *cngc2-3* throughout this work except for the Ca2+ imaging analysis (see FRET-based Ca^{2+} analysis using YC-Nano65 section).

Identification of *rdd1* as an allele of *YUC6*

The Illumina HiSeq 1500 system (Illumina, Inc., San Diego, CA, USA) at the McMaster Institute for Molecular Biology and Biotechnology (MOBIX) was used to sequence the genomic DNA extracted from leaves of 4-week-old *rdd1 cngc2-3* and *cngc2-3* plants. DNA was extracted from 100 mg of powdered leaf tissue using the cetyl trimethylammonium bromide (CTAB) method (Thompson, 1980) with a slight

modification: 200 U·mL^{-1} of RNAse A and 0.4 g·mL^{-1} PVP (MW 40,000; Sigma-Aldrich, Canada) were added to the CTAB extraction buffer. Extracted DNA was precipitated twice with isopropanol, once with 75% EtOH (v/v) and resuspended in 0.1X TE buffer supplemented with 0.2 units of RNAse A. DNA integrity was assessed using agarose gel electrophoresis and quantified with a Quant-iT PicoGreen dsDNA Assay Kit (Thermo Fisher Scientific) on a Bio-Tek Powerwave HT microplate reader. Multiplex libraries were prepared according to the manufacturer's instructions (Nextera) and the three libraries were sequenced on one flow-cell lane in high throughput mode. Raw sequence reads were trimmed for adaptor sequences with Cutadapt software (Martin, 2011) and unpaired reads, and those of length <36 nt were excluded from further analyses. Paired reads were aligned against the TAIR10 WT reference genome using BWA (Li and Durbin, 2009), and sequence variants were detected with the mpileup function of SAMtools (Li et al., 2009).

GUS enzymatic assay

Seedlings were grown on 1/2 MS, 1% sucrose (w/v), and 0.8% (w/v) agar plates for 6 d before being transferred to plates supplemented with 1-µM IAA, or solvent alone (ethanol at final concentration of 0.09% (v/v)), for 24 h. GUS reporter activity was analyzed at an excitation wavelength of 365 nm and emission wavelength of 455 nm, using a TECAN plate reader (every 10 min for 2 h) in the presence of 4-methylumbelliferyl glucuronide. GUS activity was standardized against protein concentration and data were reported as GUS activity in pmol 4-methylumbelliferone per microgram protein.

Pathogen infection

Infection with *Hyaloperonospora arabidopsidis* isolate Noco, which is virulent to the WT accession of Arabidopsis was performed as described previously with 5×10^5 spores·mL^{-1} (Chin et al., 2013).

Analysis of endogenous SA

Endogenous SA was analyzed using the *Acinetobacter* sp. ADPWH lux-based biosensor as previously described (Defraia et al., 2008).

Gravitropic root bending

Five to seven-day-old seedlings were photographed every 2 h between 4 and 10 h, and then again at 24 h, from the start of gravistimulation. The deviation in root tip angle from 90° was analyzed using the angle tool on ImageJ software (http://rsbweb.nih.gov/ij/).

Analysis of flowering transition time

Arabidopsis WT and mutant plants were grown on Sunshine-Mix #1 (Sun Gro Horticulture, Vancouver, Canada) in a growth chamber under a 16-h photoperiod (16-h light/ 8-h dark) at 22°C/18°C. Observations were made every other day and floral transition was recorded as days for the first bolt to form from time of sowing as described in Fortuna et al. (2015).

DII-VENUS analysis

For DII-VENUS analysis, seedlings were visualized for 20 min immediately after supplementation with 1-µM IAA. Confocal images were captured using a Leica TCS SP8 confocal system with an acousto-optical beam splitter; HCX PL APO CS 40x immersion oil objective; numerical aperture, 1.25; excitation: 514 nm set to 20% intensity, emission: 525–600 nm; 800 gain (Leica Microsystems). Seven- to nine-day-old seedlings were stained with 1× propidium iodide and imaged at 40× magnification. Images were processed using Leica Las AF lite software.

FRET-based Ca^{2+} analysis using YC-Nano65

Multiple lines of WT, *dnd1*, and *rdd1 dnd1* carrying YC-Nano65 were generated as previously described (Choi et al., 2014). These plants were grown on the surface of a vertical agar plate with 1/2 MS, 1% (w/v) sucrose, and 0.5% gellan gum (w/v) at pH 5.8 under ambient light conditions. The root tips were treated with 10 µL of 1-µM IAA. FRET (cpVenus) and Cyan Fluorescent Protein (CFP) signals from YC-Nano65 were acquired using a motorized fluorescence stereo microscope (SMZ-25, Nikon) equipped with image splitting optics (W-VIEW GEMINI, Hamamatsu Photonics) and a sCMOS camera (ORCA-Flash4.0 V2, Hamamatsu Photonics) as previously described (Lenglet et al., 2017; Toyota et al., 2018). For high-resolution confocal Ca^{2+} analysis, the transgenic plants were grown vertically under a thin layer (~2 mm) of the growth medium (1/2 MS, 1% (w/v) sucrose and 0.5% gellan gum (w/v) at pH 5.8) on a cover glass (24 × 50 mm, Fisher Scientific) for 6 d at 23°C. The tip of the root was exposed by removing a small window (~500 µm × 500 µm) from the gel, and 10 µL of 1-µM IAA was applied to the root tip area through this window. FRET (cpVenus) and CFP signals from YC-Nano65 were acquired using a laser scanning confocal microscope (LSM780/Elyra; Newcomb Imaging Center, Department of Botany, University of Wisconsin, Madison) as previously described (Choi et al., 2014). The cpVenus/CFP ratio was calculated using 6D imaging and Ratio & FRET plug-in modules, and the kymograph of the entire root was generated over 240 s (NIS-Elements AR, Nikon).

Statistical analyses

Microsoft Excel was used to perform Student's *t* test to compare means and generate standard error at a significance level of $P = 0.05$. Statistical significance was also confirmed using one-way analysis of variance. Tukey's honestly significant difference pairwise comparison at a significance level of $P = 0.05$ was used to generate pairwise comparisons where applicable (IBM SPSS Statistics package, version 27.0).

Accession numbers

Sequence data from this article can be found in the EMBL/ GenBank data libraries under accession number(s): *CNGC2* (AT5G15410), *RDD1/YUC6* (AT5G25620), *TAA1* (AT1G70560).

Supplemental data

The following materials are available in the online version of this article.

Supplemental Figure S1. Reverse transcription quantitative PCR analysis of At5G24680, At5G25590, and At5G26050.

Supplemental Figure S2. *rdd1* and *yuc6* are semi-dominant mutations.

Supplemental Figure S3. SA levels in *yu6* mutants are WT-like.

Supplemental Figure S4. Cold water-mediated Ca^{2+} signals is intact in *cngc2*.

Supplemental Figure S5. *cngc14* exhibits a similar degree of alterations in gravitropic root bending and distinct expression patterns from *cngc2*.

Supplemental Table S1. Segregation analysis of *yuc6-1D* and *cngc2* cross progenies.

Supplemental Table S2. Segregation analysis of progeny from crossing *yuc6 cngc2* and *cngc2*.

Supplemental Table S3. Segregation analysis of progeny from crossing *rdd1-1 cngc2* and *cngc2*.

Supplemental Table S4. Primers used in this study.

Supplemental Video S1. Ca^{2+} signal activation upon IAA treatment in Col-wt.

Supplemental Video S2. Ca^{2+} signal activation upon IAA treatment in *cngc2*.

Supplemental Video S3. Ca^{2+} signal activation upon IAA treatment in *rdd1 cngc2*.

References

Ali R, Ma W, Lemtiri-Chlieh F, Tsaltas D, Leng Q, von Bodman S, Berkowitz GA (2007) Death don't have no mercy and neither does calcium: Arabidopsis CYCLIC NUCLEOTIDE GATED CHANNEL 2 and innate immunity. Plant Cell **19**: 1081–1095

Balagué C, Lin B, Alcon C, Flottes G, Malmström S, Köhler C, Neuhaus G, Pelletier G, Gaymard F, Roby D (2003) HLM1, an essential signaling component in the hypersensitive response, is a member of the cyclic nucleotide–gated channel ion channel family. Plant Cell **15**: 365–379

Brost C, Studtrucker T, Reimann R, Denninger P, Czekalla J, Krebs M, Fabry B, Schumacher K, Grossmann G, Dietrich P (2019) Multiple cyclic nucleotide-gated channels coordinate calcium oscillations and polar growth of root hairs. Plant J **99**: 910–923

Brunoud G, Wells DM, Oliva M, Larrieu A, Mirabet V, Burrow AH, Beeckman T, Kepinski S, Traas J, Bennett MJ, et al. (2012). A novel sensor to map auxin response and distribution at high spatio-temporal resolution. Nature **482**: 103–106

Cao X, Yang H, Shang C, Ma S, Liu L, Cheng J (2019) The roles of auxin biosynthesis YUCCA gene family in plants. Int J Mol Sci **20**: 8–10

Cha J-Y, Kim MR, Jung IJ, Kang SB, Park HJ, Kim MG, Yun D-J, Kim W-Y (2016) The thiol reductase activity of YUCCA6 mediates delayed leaf senescence by regulating genes involved in auxin redistribution. Front Plant Sci **7**: 1–10

Cha JY., Kim WY, Kang SB, Kim JI, Baek D, Jung IJ, Kim MR, Li N, Kim HJ, Nakajima M, et al. (2015) A novel thiol-reductase activity of Arabidopsis YUC6 confers drought tolerance independently of auxin biosynthesis. Nature Commun **6**: 1–13

Chan C, Schorrak LM, Smith RK, Bent AF, Sussman MR (2003) A cyclic nucleotide-gated ion channel, CNGC2, is crucial for plant development and adaptation to calcium stress. Plant Physiol **132**: 728–731

Chan C, Wohlbach DJ, Rodesch MJ, Sussman MR (2008) Transcriptional changes in response to growth of Arabidopsis in high external calcium. FEBS Lett **582**: 967–976

Charpentier M, Sun J, Martins TV, Radhakrishnan GV, Findlay K, Soumpourou E, Thouin J, Véry AA, Sanders D, Morris RJ, et al. (2016) Nuclear-localized cyclic nucleotide-gated channels mediate symbiotic calcium oscillations. Science **352**: 1102–1105

Cheng Y, Dai X, Zhao Y (2006) Auxin biosynthesis by the YUCCA flavin monooxygenases controls the formation of floral organs and vascular tissues in Arabidopsis. Genes Dev **20**: 1790–1799

Cheng Y, Dai X, Zhao Y (2007) Auxin synthesized by the YUCCA flavin monooxygenases is essential for embryogenesis and leaf formation in Arabidopsis. Plant Cell **19**: 2430–2439

Chin K, DeFalco TA, Moeder W, Yoshioka K (2013) The Arabidopsis cyclic nucleotide-gated ion channels AtCNGC2 and AtCNGC4 work in the same signaling pathway to regulate pathogen defense and floral transition. Plant Physiol **163**: 611–624

Choi W-G, Toyota M, Kim S-H, Hilleary R, Gilroy S (2014) Salt stress-induced Ca2+ waves are associated with rapid, long-distance root-to-shoot signaling in plants. Proc Natl Acad Sci **111**: 6497–6502

Chou H, Zhu Y, Ma Y, Berkowitz GA (2016) The CLAVATA signaling pathway mediating stem cell fate in shoot meristems requires Ca2+ as a secondary cytosolic messenger. Plant J **85**: 494–506

Clough SJ, Fengler KA, Yu IC, Lippok B, Smith RK, Bent AF (2000) The Arabidopsis dnd1 "defense, no death" gene encodes a mutated cyclic nucleotide-gated ion channel. Proc Natl Acad Sci **97**: 9323–9328

DeFalco TA, Bender KW, Snedden WA (2010) Breaking the code: Ca2+ sensor in plant signaling. Biochem J **425**: 27–40

DeFalco TA, Moeder W, Yoshioka K (2016) Opening the gates: insights into cyclic nucleotide-gated channel-mediated signaling. Trends Plant Sci **21**: 903–906

Defraia CT, Schmelz EA, Mou Z (2008) A rapid biosensor-based method for quantification of free and glucose-conjugated salicylic acid. Plant Methods **4**: 1–11

Demidchik V, Shabala S, Isayenkov S, Cuin TA, Pottosin I (2018) Calcium transport across plant membranes: mechanisms and functions. New Phytol **220**: 49–69

Dietrich P, Moeder W, Yoshioka K (2020) Plant Cyclic Nucleotide-Gated Channels: New Insights on Their Functions and Regulation. Plant Physiol **184**: 27–38

Dindas J, Scherzer S, Roelfsema MRG, Von Meyer K, Müller HM, Al-Rasheid KAS, Palme K, Dietrich P, Becker D, Bennett MJ, et al. (2018) AUX1-mediated root hair auxin influx governs SCFTIR1/AFB-type Ca2+ signaling. Nat Commun **9**: 1174

Edel KH, Marchadier E, Brownlee C, Kudla J, Hetherington AM (2017) The evolution of calcium-based signalling in plants. Curr Biol **27**: R667–R679

Fichman Y, Myers RJ, Grant DAG, Mittler R (2021) Plasmodesmata-localized proteins and ROS orchestrate light-induced rapid systemic signaling in Arabidopsis. Sci Signal **14**: 36–38

Finka A, Cuendet AFH, Maathuis FJM, Saidi Y, Goloubinoff P (2012) Plasma membrane cyclic nucleotide gated calcium channels control land plant thermal sensing and acquired thermotolerance. Plant Cell **24**: 3333–3348

Fortuna A, Lee J, Ung H, Chin K, Moeder W, Yoshioka K (2015) Crossroads of stress responses, development and flowering regulation—the multiple roles of cyclic nucleotide gated ion channel 2. Plant Signal Behav **10**: 23–26

Genger RK, Jurkowski GI, Mcdowell JM, Lu H, Jung HW, Greenberg JT, Bent AF, Pathology P, Madison W (2008) Signaling pathways that regulate the enhanced disease resistance of Arabidopsis "defense, no death" mutants. Mol Plant Microbe Interact **21**: 1285–1296

Jammes F, Hu HC, Villiers F, Bouten R, Kwak JM (2011) Calcium-permeable channels in plant cells. FEBS J **278**: 4262–4276

Jurkowski GI, Smith RK, Yu I, Ham JH, Sharma SB, Klessig DF, Fengler Ka, Bent AF (2004) Arabidopsis DND2, a second cyclic nucleotide-gated ion channel gene for which mutation causes the "defense, no death" phenotype. Mol Plant Microbe Interact **17**: 511–520

Kale L, Nakurte I, Jalakas P, Kunga-Jegere L, Brosché M, Rostoks N (2019) Arabidopsis mutant dnd2 exhibits increased auxin and abscisic acid content and reduced stomatal conductance. Plant Physiol Biochem **140**: 18–26

Kazan K, Lyons R (2014) Intervention of phytohormone pathways by pathogen effectors. Plant Cell **26**: 2285–2309

Kim JI, Sharkhuu A, Jin JB, Li P, Jeong JC, Baek D, Lee SY, Blakeslee JJ, Murphy AS, Bohnert HJ, et al. (2007) yucca6, a dominant mutation in Arabidopsis, affects auxin accumulation and auxin-related phenotypes. Plant Physiol **145**: 722–735

Kim JI, Murphy AS, Baek D, Lee SW, Yun DJ, Bressan RA, Narasimhan ML (2011) YUCCA6 over-expression demonstrates auxin function in delaying leaf senescence in Arabidopsis thaliana. J Exp Bot **62**: 3981–3992

Kunkel BN, Harper CP (2018) The roles of auxin during interactions between bacterial plant pathogens and their hosts. J Exp Bot **69**: 245–254

Lemtiri-Chlieh F, Berkowitz GA (2004) Cyclic adenosine monophosphate regulates calcium channels in the plasma membrane of Arabidopsis leaf guard and mesophyll cells. J Biol Chem **279**: 35306–35312

Lenglet A, Jaslan D, Toyota M, Mueller M, Thomas M, Schonknecht G, Marten I, Gilroy S, Hedrich R, Farmer EE (2017) Control of basal jasmonate signalling and defence through modulation of intracellular cation flux capacity. New Phytol **216**: 1161–1169

Leyser O (2018) Auxin Signaling. Plant Physiol **176**: 465–479

Li H, Durbin R (2009) Fast and accurate short read alignment with Burrows–Wheeler transform. Bioinformatics **25**: 1754–1760

Li H, Handsaker B, Wysoker A, Fennell T, Ruan J, Homer N, Marth G, Abecasis G, Durbin R, Data GP, et al. (2009) The sequence alignment/map format and SAMtools. Bioinformatics **25**: 2078–2079

Martin M (2011) Cutadapt removed adapter sequences from high-throughput sequencing read. EMBnet J **17**: 5–7

Mashiguchi K, Tanaka K, Sakai T, Sugawara S, Kawaide H, Natsume M, Hanada A, Yaeno T, Shirasu K, Yao H, et al. (2011) The main auxin biosynthesis pathway in Arabidopsis. Proc Natl Acad Sci **108**: 18512–18517

Moeder W, Phan V, Yoshioka K (2019) Ca2+ to the rescue – Ca2+ channels and signaling in plant immunity. Plant Sci **279**: 19–26

Moeder W, Urquhart W, Ung H, Yoshioka K (2011) The role of cyclic nucleotide-gated ion channels in plant immunity. Mol Plant **4**: 442–452

Monshausen GB, Miller ND, Murphy AS, Gilroy S (2011) Dynamics of auxin-dependent Ca2+ and pH signaling in root growth revealed by integrating high-resolution imaging with automated computer vision-based analysis. Plant J **65**: 309–318

Mutka AM, Fawley S, Tsao T, Kunkel BN (2013) Auxin promotes susceptibility to Pseudomonas syringae via a mechanism independent of suppression of salicylic acid-mediated defenses. Plant J **74**: 746–754

Pan Y, Chai X, Gao Q, Zhou L, Zhang S, Li L, Luan S (2019) Dynamic interactions of plant CNGC subunits and article dynamic interactions of plant CNGC subunits and calmodulins drive oscillatory Ca2+ channel activities. Dev Cell **48**: 710–725.e5

Shih HW, Depew CL, Miller ND, Monshausen GB (2015) The cyclic nucleotide-gated channel CNGC14 regulates root gravitropism in Arabidopsis thaliana. Curr Biol **25**: 3119–3125

Somssich M, Je Il B, Simon R, Jackson D (2016) CLAVATA-WUSCHEL signaling in the shoot meristem. Development **143**: 3238–3248

Stepanova AN, Robertson-hoyt J, Yun J, Benavente LM, Xie D, Dole K, Schlereth A, Ju G, Alonso JM (2008) TAA1-mediated auxin biosynthesis is essential for hormone crosstalk and plant development. Cell **133**: 177–191

Stepanova AN, Yun J, Robles LM, Novak O, He W, Guo H, Ljung K, Alonso JM (2011) The *Arabidopsis* YUCCA1 flavin monooxygenase functions in the indole-3-pyruvic acid branch of auxin biosynthesis. Plant Cell **23**: 3961–3973

Thompson WF (1980) Rapid isolation of higher weight plant DNA. Nucleic Acids Res **8**: 4321–4325

Tian W, Hou C, Ren Z, Wang C, Zhao F, Dahlbeck D, Hu S, Zhang L, Niu Q, Li L, et al. (2019) A calmodulin-gated calcium channel links pathogen patterns to plant immunity. Nature **572**: 131–135

Toyota M, Spencer D, Sawai-toyota S, Jiaqi W, Zhang T, Koo A, Howe G, Gilroy S (2018) Glutamate triggers long-distance, calcium-based plant defense signaling. Science **6**: 1112–1115

Ulmasov T, Murfett J, Hagen G, Guilfoyle TJ (1997) Aux/IAA proteins repress expression of reporter genes containing natural and highly active synthetic auxin response elements. Plant Cell **9**: 1963–1971

Urquhart W, Gunawardena AHLAN, Moeder W, Ali R, Berkowitz GA, Yoshioka K (2007) The chimeric cyclic nucleotide-gated ion channel ATCNGC11/12 constitutively induces programmed cell death in a Ca2+ dependent manner. Plant Mol Biol **65**: 747–761

Vanneste S, Friml J (2009) Auxin: a trigger for change in plant development. Cell 136: 1005–1016

Waadt R, Krebs M, Kudla J, Schumacher K (2017) Multiparameter imaging of calcium and abscisic acid and high-resolution quantitative calcium measurements using R-GECO1-mTurquoise in Arabidopsis. New Phytol **216**: 303–320

Wang D, Pajerowska-Mukhtar K, Culler AH, Dong X (2007) Salicylic acid inhibits pathogen growth in plants through repression of the auxin signaling pathway. Cur Biol **17**: 1784–1790

Wang Q, Qin G, Cao M, Chen R, He Y, Yang L, Zeng Z, Yu Y, Gu Y, Xing W, et al. (2020) A phosphorylation-based switch controls TAA1-mediated auxin biosynthesis in plants. Nat Commun **11**: 1–10

Wang Y, Kang Y, Ma C, Miao R, Wu C, Long Y, Ge T, Wu Z, Hou X, Zhang J, Qi Z (2017) CNGC2 is a Ca2+ influx channel that prevents accumulation of apoplastic Ca2+ in the leaf. Plant Physiol **173**: 1342–1354

Won C, Shen X, Mashiguchi K, Zheng Z, Dai X, Cheng Y, Kasahara H (2011) Conversion of tryptophan to indole-3-acetic acid by TRYPTOPHAN AMINOTRANSFERASES OF ARABIDOPSIS and YUCCAs in Arabidopsis. Proc Natl Acad Sci **108**: 18518–18523

Yoshioka K, Moeder W, Kang H-G, Kachroo P, Masmoudi K, Berkowitz G, Klessig DF (2006) The chimeric Arabidopsis CYCLIC NUCLEOTIDE-GATED ION CHANNEL11/12 activates multiple pathogen resistance responses. Plant Cell **18**: 747–763

Yu IC, Parker J, Bent AF (1998) Gene-for-gene disease resistance without the hypersensitive response in Arabidopsis dnd1 mutant. Proc Natl Acad Sci **95**: 7819–7824

Yuan P, Jauregui E, Du L, Tanaka K, Poovaiah BW (2017) Calcium signatures and signaling events orchestrate plant–microbe interactions. Curr Opin Plant Biol **38**: 173–183

Zelman AK, Dawe A, Gehring C, Berkowitz GA, Murphy AS, Schoenknecht G, Blakeslee J (2012) Evolutionary and structural perspectives of plant cyclic nucleotide-gated cation channels. Front Plant Sci **3**: 1–13

Zhou Z, Zhang C, Wu L, Zhang C, Chai J, Wang M, Jha A, Jia P, Cui S, Yang M, et al. (2011) Functional characterization of the CKRC1/TAA1 gene and dissection of hormonal actions in the Arabidopsis root. Plant J **66**: 516–527